Bulk motion-independent analyses of water diffusion changes in the brain during the cardiac cycle

著者	Nakamura Tomoya, Miyati Tosiaki, Kasai Harumasa, Ohno Naoki, Yamada Masato, Mase Mitsuhito, Hara Masaki, Shibamoto Yuta, Suzuki Yuriko, Ichikawa Katsuhiro
journal or publication title	Radiological Physics and Technology
volume	2
number	2
page range	133-137
year	2009-07-01
URL	http://hdl.handle.net/2297/19320

doi: 10.1007/s12194-009-0056-3

Title:

Bulk-motion-independent analyses of water diffusion change in the brain during the cardiac cycle

Author's Names and Degrees:

Tomoya Nakamura, MS, [1] Tosiaki Miyati, PhD, DMSc, [2] Harumasa Kasai, BS, [3] Naoki Ohno, BS, [2] Masato Yamada, BS, [3] Mitsuhito Mase, MD, PhD, [4] Masaki Hara, MD, PhD, [3] Yuta Shibamoto, MD, PhD, [3] Yuriko Suzuki, BS, [5] Katsuhiro Ichikawa, PhD, [2]

Author Affiliations:

[1]Department of Radiology, Tokai University Hachioji Hospital, 1838 Ishikawa-machi, Hachioji, 192-0032, Japan

[2]Division of Health Sciences, Graduate School of Medical Science, Kanazawa University, 5-11-80 Kodatsuno, Kanazawa, 920-0942, Japan

[3]Department of Radiology, Nagoya City University Hospital, 1 Kawasumi, Mizuho-machi, Mizuho-ku, Nagoya, 467-8602, Japan

[4]Department of Neurosurgery and Restorative Neuroscience, Nagoya City University Graduate School of Medical Sciences, 1 Kawasumi, Mizuho-machi, Mizuho-ku, Nagoya, 467-8601, Japan

[5]MR Clinical Science, Philips Medical Systems, 2-13-37 Kounan, Minato-ku, 108-8507, Japan

Corresponding Author and Reprint Info:

Tomoya Nakamura

Department of Radiology, Tokai University Hachioji Hospital

1838 Ishikawa-machi, Hachioji, 192-0032, Japan

Email address: nakamura.tomoya@hachioji-hosp.tokai.ac.jp

Phone number: +81-426-39-1111

Fax number: +81-426-39-1112

A Concise and Informative Title:

Bulk-motion-independent analyses of water diffusion change

Bulk-motion-independent analyses of water diffusion change in the brain during the cardiac cycle

Abstract

We evaluated dynamic changes in water diffusion in the brain during the cardiac cycle by using cine diffusion MRI. On a 1.5-T MRI, ECG-triggered single-shot diffusion echo planar imaging was used with sensitivity encoding, halfscan, and rectangular field of view techniques for minimizing bulk motion effects such as brain pulsation, with a data-sampling window of 3 ms. The apparent diffusion coefficient (ADC) and fractional anisotropy (FA) in the white matter zone were determined in ten healthy volunteers and then compared with the intracranial volume change (ICVC) determined by phase-contrast cine MRI during the cardiac cycle. Moreover, a frequency analysis of these waveforms was performed. ADC and FA values changed significantly during the cardiac cycle, despite minimizing the effect of bulk motion, i.e., independent of the bulk motion. The ADC was synchronized with the ICVC during the cardiac cycle. A significant positive correlation was noted among their amplitudes. Analysis of the dynamic change of water diffusion by use of cine diffusion MRI facilitates the assessment of intracranial conditions.

Keywords: diffusion; bulk motion; apparent diffusion coefficient (ADC); fractional anisotropy (FA); intracranial volume change (ICVC)

1 Introduction

Recently, diffusion magnetic resonance imaging (MRI) of the brain has been shown to have significant clinical relevance for both the early detection of infarcts and other pathologic conditions [1, 2]. However, there have been problems due to main field inhomogeneity and the motion effect [3]. The former problem was solved by parallel imaging such as sensitivity encoding (SENSE) [4] or periodically rotated overlapping parallel lines with enhanced reconstruction [5]. Concerning the phase dispersion caused by the bulk motion effect of brain pulsation [6-9], Brockstedt et al. [9], who used single-shot echo planar imaging (EPI), reported that the apparent diffusion coefficient (ADC) was not significantly altered during the cardiac cycle. However, they evaluated only two delay times (100 ms, 400 ms) during the cardiac cycle. On the other hand, it has been reported that brain pulsation can give rise to artifactual signal attenuation leading to over-estimation of the ADC [10-13].

In this study, we precisely evaluated dynamic changes in water diffusion during the cardiac cycle by using ECG-triggered single-shot diffusion EPI with high temporal resolution and instantaneous data sampling to minimize the bulk motion

effect. Furthermore, we measured volume loading of the cranium, i.e., the net intracranial volume change (ICVC) [14, 15] with phase-contrast (PC) cine MRI during the cardiac cycle, and we calculated the phase difference among the main wave components of ADC, fractional anisotropy (FA), and ICVC by Fourier analysis.

2 Materials and Methods

2.1 Procedure for calculating ADC and FA during the cardiac cycle

EPI is a well-established technique for diffusion MRI of the brain because it is insensitive to motion [16]. In particular, single-shot EPI is largely insensitive to motion. However, it is difficult to eliminate the bulk motion effect completely by using single-shot EPI alone; thus, we used SENSE, half-Fourier, and rectangular field of view (FOV) techniques (see Section 2.4, Imaging conditions) to minimize the bulk motion effect, i.e., a data-sampling window of approximately 3 ms, and we evaluated dynamic changes in water diffusion during the cardiac cycle.

First, the ADC and FA maps were calculated from ECG-triggered single-shot

diffusion EPI images (8 cardiac phases) during the cardiac cycle with Equations (1) and (2) (Fig. 1a and b):

$$ADC = \frac{\ln(S_1 / S_2)}{b_2 - b_1} \quad (1)$$

$$FA = \sqrt{\frac{3}{2}} \frac{\sqrt{(\lambda_1 - D)^2 + (\lambda_2 - D)^2 + (\lambda_3 - D)^2}}{\sqrt{\lambda_1^2 + \lambda_2^2 + \lambda_3^2}}, \quad (2)$$

where b_1 and b_2 represent the b factor of 0 and 1000 s/mm^2, and S_1 and S_2 represent the signal intensities at each b value, respectively. λ_1, λ_2, and λ_3 represent the eigenvalues of the principal, medium, and minor eigenvectors, and D represents the trace $(\lambda_1 + \lambda_2 + \lambda_3)/3$ of the diffusion tensor. Next, we obtained high-contrast and high-resolution T1 and T2 images at the same slice, and a region-of-interest (ROI) was established (Fig. 1c) in the white matter by subtraction of T2 images from T1 images for improvement of the image contrast between white matter and gray matter. Then we set the ROI on the cerebral white matter and determined the mean ADC and FA values in each cardiac phase. The statistical difference between the maximum ADC or FA phase and the minimum phase was determined by two-sided paired *t* test.

2.2 Procedure for calculating ICVC during the cardiac cycle

We first set the slice plane at the dense (C2) level, and obtained (see Section 2.4, Imaging conditions) velocity-mapped phase images twice (32 cardiac phases) with different velocity-encoding gradients for cerebrospinal fluid (CSF) flow and cord motion as well as for transcranial blood flow [14, 15]. To obtain the net transcranial flow, we measured the flow (or displacement) during the cardiac cycle in each region; CSF flow [$V_c(t)$], displacement of cord [$V_s(t)$], arterial inflow (both internal carotid arteries and both vertebral arteries) [$V_a(t)$], and venous outflow (both internal jugular veins) [$V_v(t)$]. Next, we corrected the baseline offset due to eddy currents by using a subtraction process [17]. Then, for matching the difference in inflow and outflow capacity to the cranium during the cardiac cycle, the flow wave of the venous outflow was scaled up, and the ICVC [*ICVC* (*t*)] in each cardiac phase was calculated from Equation (3):

$$ICVC(t) = \int [V_a(t) + V_v(t) + V_c(t) + V_s(t)]\,dt \quad , \quad (3)$$

where the measured volumetric flow in each region was positive in the cranial direction. For details of these measurements, see Refs. 14 and 15.

2.3 Fourier analysis

Phase differences between the highest-amplitude harmonic of ADC, FA, and ICVC waves during the cardiac cycle were compared by Fourier analysis. Moreover, the amplitude of ADC, FA, and ICVC waves during the cardiac cycle were compared with each harmonic; the number of phases of ADC and FA was interpolated to 32 phases.

2.4 Imaging conditions

MRI was performed on a 1.5T Gyroscan Intera (Philips Medical Systems International, Best, The Netherlands). Scan parameters of spin echo-ECG-triggered multislice multi-phase single-shot diffusion EPI with spectral presaturation with inversion recovery sequence were set as follows: shortest TE = 70 ms, FOV = 256 mm, imaging matrix = 64×64, slice thickness = 4 mm, number of cardiac phases = 8, flip angle = 90 degrees, number of slices = 5-20, b factor = 0 and 1000 s/mm^2, SENSE factor = 2, halfscan factor = 0.75, number of signals averaged (NSA) = 1, phase encoding = right/left, and diffusion gradient = 6 axes.

In addition, scan parameters of the retrospective cardiac gated PC cine MRI sequence were set: shortest TE = 20 ms, FOV = 140 mm, imaging matrix =

256×128, slice thickness = 5 mm, number of cardiac phases = 32, flip angle = 20 degrees, number of slices = 1, with flow compensation, velocity encoding for blood flow = ±70 cm/s, velocity encoding for CSF and cord flow = ±7 cm/s, NSA = 1, and phase encoding = right/left.

Ten healthy human volunteers were examined for seven men and three women, 22-46 years. Informed consent was obtained prior to the examination.

3 Results

The maximum ADC of the cerebral white matter zone during the cardiac cycle was 0.778 ± 0.033, and the minimum ADC of the cerebral white matter zone during the cardiac cycle was 0.708 ± 0.026 (Table 1). ADC values in the cerebral white matter zone changed significantly during the cardiac cycle (P = 0.01) (Fig. 2).

The maximum FA of the cerebral white matter zone during the cardiac cycle was 0.440 ± 0.039, and the minimum FA of the cerebral white matter zone during the cardiac cycle was 0.358 ± 0.048 (Table 1). FA values in the cerebral white

matter zone also changed significantly during the cardiac cycle (P = 0.01) (Fig. 2).

Phase differences between main wave components (1st, 2nd, 3rd, or 4th harmonic) of ADC, FA, and ICVC during the cardiac cycle are shown in Fig. 3. The phase between ADC and ICVC was the same; however, FA and ICVC were inverted. Moreover, there were significant positive correlations between the amplitudes of ADC and ICVC, and FA and ICVC (r = 0.76 and r = 0.72, respectively).

4 Discussion

The ADC value in the cerebral white matter zone changed significantly during the cardiac cycle when obtained under the conditions described here in which we used instantaneous data-sampling, even though, Brockstedt et al. [9] reported that the ADC value was not changed significantly during the cardiac cycle with a single-shot EPI sequence. However, there was no constant relationship among these maximum or minimum peak times from the R-wave. Thus, it is difficult to evaluate the change in ADC during the cardiac cycle by analyzing the two delay

times between R-peaks in the cardiac cycle. It is considered that ICVC, i.e., regional volume loading, makes the water molecules fluctuate, rather than the bulk motion or perfusion effect during the cardiac cycle, because we used an instantaneous data-sampling time or a high b value [18]. Moreover, the waveform of the ADC in the cardiac cycle was similar to that of the ICVC: i.e., these phases were the same (Fig. 2, Fig. 3). Furthermore, as shown in Results, the amplitudes of the ADC and ICVC waves had significant positive correlations. An example of ADC, FA, and ICVC during the cardiac cycle is shown in Fig. 2.

On the other hand, the FA also changed significantly during the cardiac cycle, which caused the tractography in each cardiac phase to vary as well (Fig. 4). However, the waveform of the FA in the cardiac cycle was not similar to that of the ICVC (Fig. 2, Fig. 3). We can’t explain the exact reason for the present stage; this needs to be pursued in detail in forthcoming studies, i.e., by increases in the number of cardiac phases or reduction of the voxel size.

This dynamic change in ADC during the cardiac cycle has been considered to result in artifacts [6-13, 19-21], but that may be useful as new biomechanical information such as patients with subdural hematoma and normal pressure

hydrocephalus.

Conclusion

ADC and FA values change significantly during the cardiac cycle even if the effect of bulk motion is minimized, i.e., these changes are independent of the bulk motion. The analysis of ADC on ECG-triggered diffusion MRI makes it possible to assess water molecular motion dynamics, and to obtain a more detailed determination of the intracranial state.

References

1. Moseley ME, Cohen Y, Mintorovitch J, et al. Early detection of regional cerebral ischemia in cats: comparison of diffusion- and T2-weighted MRI and spectroscopy. Magn Reson Med 1990;14(2):330-346.

2. Mintorovitch J, Moseley ME, Chileuitt L, et al. Comparison of diffusion- and T2-weighted MRI for the early detection of cerebral ischemia and reperfusion

in rats. Magn Reson Med 1991;18(1):39-50.

3. Johnson G, Hutchison JMS. The limitations of NMR recalled-echo imaging techniques. J Magn Reson Imaging 1985;63:14-30.

4. Pruessmann KP, Weiger M, Scheidegger MB, et al. SENSE: sensitivity encoding for fast MRI. Magn Reson Med 1999;42(5):952-962.

5. Pipe JG, Farthing VG, Forbes KP. Multishot diffusion-weighted FSE using PROPELLER MRI. Magn Reson Med 2002;47(1):42-52.

6. Chenevert TL, Pipe JG. Effect of bulk tissue motion on quantitative perfusion and diffusion magnetic resonance imaging. Magn Reson Med 1991;19(2):261-265.

7. Greitz D, Wirestam R, Franck A, et al. Pulsatile brain movement and associated hydrodynamics studied by magnetic resonance phase imaging. Neuroradiol. 1992;34(5):370-380.

8. Anderson AW, Gore JC. Analysis and correction of motion artifacts in diffusion weighted imaging. Magn Reson Med. 1994;32(3):379-387.

9. Brockstedt S, Borg M, Geijer B, et al. Triggering in quantitative diffusion imaging with single-shot EPI. Acta Radiol. 1999;40(3):263-269.

10. Skare S, Andersson JL. On the effects of gating in diffusion imaging of the brain using single shot EPI. Magn Reson Imaging. 2001;19(8):1125-1128.

11. Nunes RG, Jezzard P, Clare S. Investigations of the efficiency of cardiac-gated methods for the acquisition of diffusion-weighted images. J Magn Reson Imaging 2005;177(1):102-110.

12. Robson MD, Porter DA. Reconstruction as a source of artifact in nongated single-shot diffusion-weighted EPI. Magn Reson Imaging. 2005;23:899-905.

13. Summers P, Staempfli P, Jaermann T, et al. A preliminary study of the effects of trigger timing on diffusion tensor imaging of the human spinal cord. AJNR Am J Neuroradiol. 2006;27(9):1952-1961.

14. Alperin NJ, Lee SH, Loth F, et al. MR-intracranial pressure (ICP): A method to measure intracranial elastance and pressure noninvasively by means of MR imaging. Radiology. 2000;217(3):877-885.

15. Miyati T, Mase M, Kasai H, et al. Noninvasive MRI assessment of intracranial compliance in idiopathic normal pressure hydrocephalus. J Magn Reson Imaging 2007;26(2):274-278.

16. Norris DG. Implications of bulk motion for diffusion-weighted imaging

experiments: Effects, mechanisms, and solutions. J Magn Reson Imaging 2001;13(4):486-495.

17. Thomsen C, Ståhlberg F, Stubgaard M, et al. Fourier analysis of cerebrospinal fluid flow velocities: MR imaging study. Radiology. 1990;177(3):659-665.

18. Le Bihan D, Breton E, Lallemand D, et al. Separation of diffusion and perfusion in intravoxel incoherent motion MR imaging. Radiology. 1988;168(2):497-505.

19. Feinberg DA, Mark AS. Human brain motion and cerebrospinal fluid circulation demonstrated with MR velocity imaging. Radiology. 1987;163(3):793-799.

20. Enzmann DR, Pelc NJ. Brain motion: measurement with phase-contrast MR imaging. Radiology. 1992;185(3):653-660.

21. Poncelet BP, Wedeen VJ, Weisskoff RM, et al. Brain parenchyma motion: measurement with cine echo-planar MR imaging. Radiology. 1992;185(3):645-651.

Acknowledgement

The author would like to thank the reviewers and the editorial assistants for the valuable comments and suggestions which significantly improved the presentation of this paper.

Figure legends

Fig. 1 ADC map (a) and FA map (b) during the cardiac cycle in the brain, and ROI of the white matter (c) obtained by subtraction of T2-weighted image from T1-weighted image.

Fig. 2 An example of ADC (a), FA (b), and ICVC (c) during the cardiac cycle.

Fig. 3 Phase differences between main wave components (1st, 2nd, 3rd, or 4th harmonic) of ADC, FA, and ICVC calculated by Fourier analysis.

Fig. 4 Tractography in each cardiac phase. Note that each tractography changes during the cardiac cycle (circles).

Table

Table 1 Change in ADC, FA, and ICVC during the cardiac cycle

	Cerebral white matter zone		
	ADC ($\times 10^{-3} mm^2/s$)	FA	ICVC (ml)
Maximum value	0.778 ± 0.033	0.440 ± 0.039	0.482 ± 0.296
Minimum value	0.708 ± 0.026	0.358 ± 0.048	-0.155 ± 0.201
Range of change	0.070 ± 0.027	0.082 ± 0.028	0.637 ± 0.372

(Mean ± standard deviation)

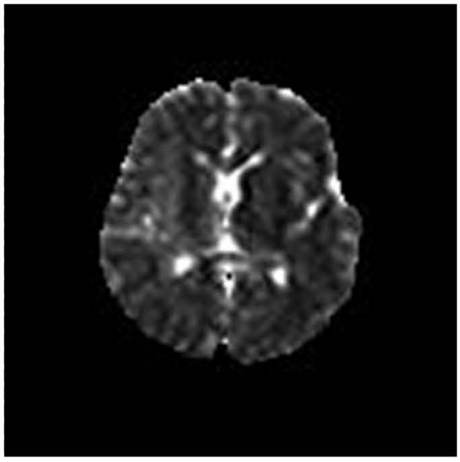

a

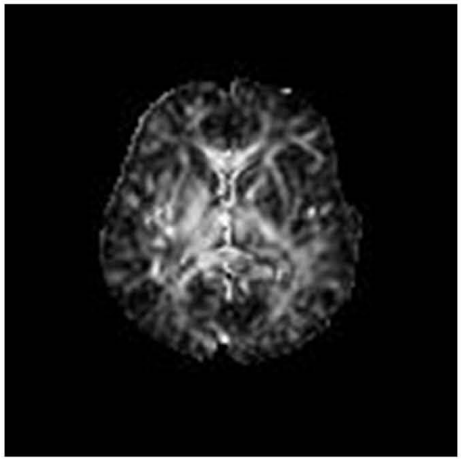

b

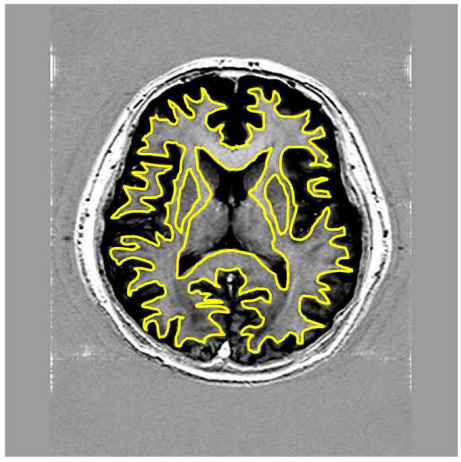

c

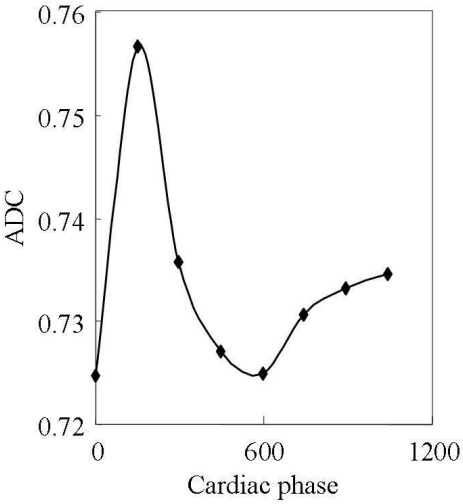
0.76
0.75
0.74
0.73
0.72
ADC
0
600
1200
Cardiac phase

a

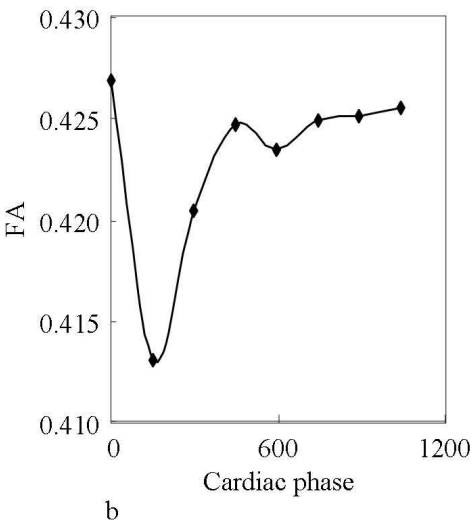
0.430
0.425
0.420
0.415
0.410
FA
0
600
1200
Cardiac phase

b

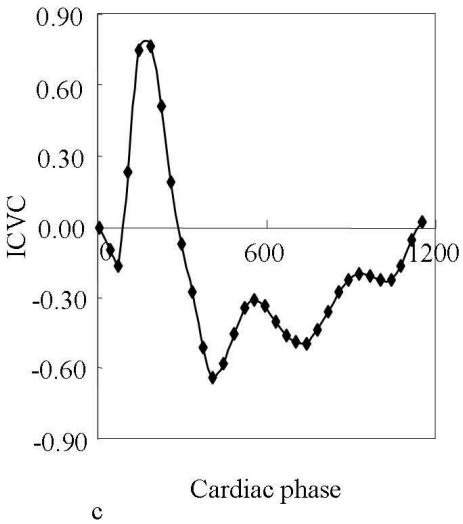
0.90
0.60
0.30
0.00
-0.30
-0.60
-0.90
ICVC
600
1200
Cardiac phase

c

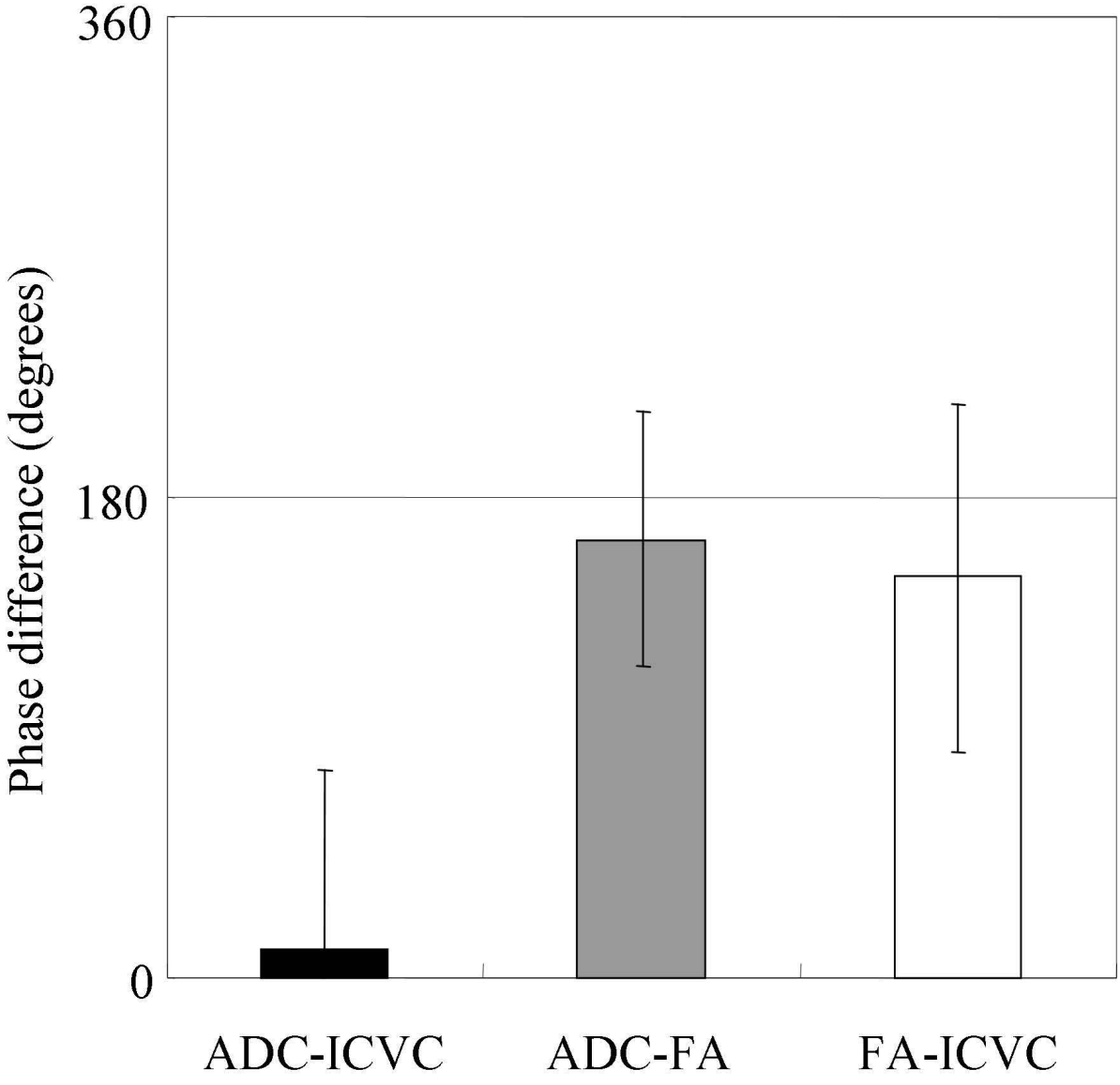
360
180
0
Phase difference (degrees)
ADC-ICVC
ADC-FA
FA-ICVC